Characterization and Modeling of a Virtual Air Gap by Means of a Reluctance Network

Jean-Francois Brudny, Guillaume Parent, Ines Naceur

▶ **To cite this version:**

Jean-Francois Brudny, Guillaume Parent, Ines Naceur. Characterization and Modeling of a Virtual Air Gap by Means of a Reluctance Network. IEEE Transactions on Magnetics, Institute of Electrical and Electronics Engineers, 2017, 53 (7), pp.8002007. 10.1109/TMAG.2017.2680402 . hal-03350733

HAL Id: hal-03350733

https://hal-univ-artois.archives-ouvertes.fr/hal-03350733

Submitted on 16 May 2022

HAL is a multi-disciplinary open access archive for the deposit and dissemination of scientific research documents, whether they are published or not. The documents may come from teaching and research institutions in France or abroad, or from public or private research centers.

L'archive ouverte pluridisciplinaire **HAL**, est destinée au dépôt et à la diffusion de documents scientifiques de niveau recherche, publiés ou non, émanant des établissements d'enseignement et de recherche français ou étrangers, des laboratoires publics ou privés.

Characterization and modeling of a virtual air gap by means of a reluctance network

Jean-François Brudny[1], Guillaume Parent[1], and Inès Naceur[1]
[1]Univ. Artois, Laboratoire Systèmes Electrotechniques et Environnement (LSEE), F-62400, Béthune, France

This paper deals with an analytical model of the virtual air gap function in order to define design rules when this technique is used inside complex devices. The establishment of those design rules constitutes the main originality of the developments presented in the paper, which are about a single phase magnetic core. It is based on the definition of a nonlinear reluctance network that takes simultaneously into account the effects of DC and AC magnetic flux components in the disturbed area that contains the virtual air gap. The results are validated using a finite element analysis and experimentally.

***Index Terms*—Magnetic core, saturation, virtual air gap, variable inductance, magnetic equivalent circuit.**

I. Introduction

THE Virtual Air Gap (VAG) concept has been introduced in order to control the transformer inrush currents [1]. Since then, this technique has been taken up in North America [2]–[5]. The principle consists in arranging auxiliary windings inside a magnetic core excited by a DC current in order to generate variable local saturations. These saturations modify the R_{MC} core reluctance seen from a main winding wounded on the magnetic core and supplied by an AC voltage source. That way, this magnetic core can be assimilated to a regular one including a mechanical air gap with a variable thickness g. Seen from the AC voltage source, the operation of the VAG can also be seen as a variable inductance L^{p}. Due to the complexity of the magnetic phenomena occurring around the auxiliary windings the VAG behavior is usually studied by finite element analysis, although investigations were conducted to provide analytical characterizations [6]. Recently, two patents involving the VAG, in partnership with EDF R&D, were published. The first one [7] concerns a series current limiter allowing to monitor the inrush current of induction machines directly connected to the electrical grid. More generally, it allows to limit the short-circuit currents in power grids. This aspect can be particularly advantageous when the power demanded by certain installations connected to this network increases. Indeed, in this case, this limiter makes it possible to minimize the costs generated by the necessary structural modifications, such as changing the transformer, without being obliged to change the upstream protective device. The second pattern [8] is about the Dynamic Voltage Restorers, more especially the protection of their static power converter parts [9,10].

Note that the local aspect characterizing the nonlinear effects of the VAG leads to an interesting property: it is possible to use several VAG on one magnetic core in order to obtain a global effect equal to the sum of those produced by each VAG. This property can be very usefull when designing a device in which a significant VAG effect is required.

In order to define preliminary design rules, this paper establishes a model to analytically characterize the function provided by the VAG under stady-state operating conditions with sinusoidal supply for the main winding. First, the studied device is introduced. Then, an analytical modeling based on a nonlinear reluctance network [11] is reported. The third part presents several waveforms, deduced from a simple spreadsheet, characterizing the device operation. That makes it possible to formulate relationships representing the VAG behavior leading to a very easy characterization of auxiliary winding design, which constitute the main contribution of this paper. Finally, relevant specifications, useful for the design of such a device are presented and validated experimentally.

In the following, given a time-dependant electric or magnetic variable z, its peak value and RMS value are noted $\hat{z}$ and Z respectively.

Corresponding author: G. Parent (email: guillaume.parent@univ-artois.fr)

II. Virtual Air Gap Characterization

Fig. 1 presents a magnetic core on which a n^{p} turn main winding supplied by an AC voltage source, noted v^{p}, of frequency f, period T and angular frequency ω, is wound.

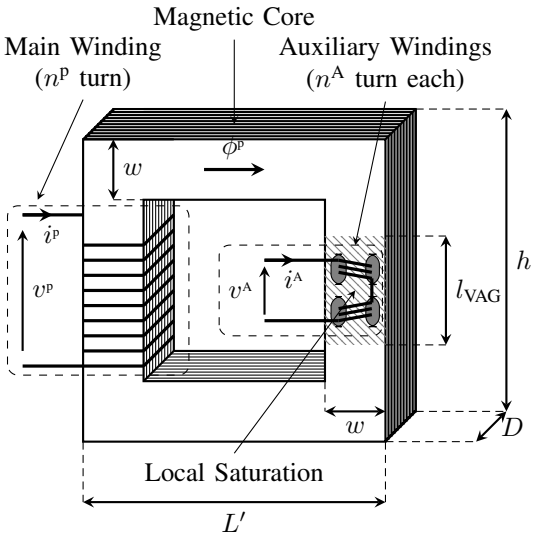

Fig. 1. Magnetic core with a virtual air gap

All the results presented in the following correspond to a sinusoidal - 50 Hz v^{p} source. The magnetic core, whose

dimensions (Fig. 1) are $L' = 164\,\text{mm}$, $h = 284\,\text{mm}$, $D = 66\,\text{mm}$ and $w = 66\,\text{mm}$, is made of an isotropic steel characterized by its first magnetization curve $b(h)$. From this curve, the variations of the relative magnetic permeability $\mu_\text{r}(b)$ are obtained and presented in Fig. 2.

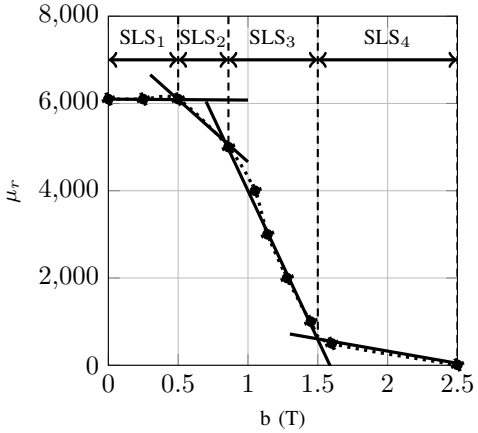

Fig. 2. Variations of relative permeability with magnetic flux density

The magnetic core is charaterized by its cross-section $S_\text{MC} = Dw$ and its mean length $L_\text{MC} = 2(L' + h - 2w)$. The local saturation of the core is achieved by two auxiliary windings of n^A turns each located in four orifices crossed by a i^A DC current. The axis of each auxiliary winding coincides with the y axis of the core. Moreover, the x axis equidistant from each auxiliary winding can be considered as magnetically neutral.

This specific geometry, which considers a small value for D with regard to w brings two advantages:

1) during conventional operation mode, i.e. $i^\text{A} = 0\,\text{A}$, it allows to limit the perturbations on the AC magnetic flux line distribution inside the magnetic core,
2) during the VAG operating mode, i.e. $i^\text{A} \neq 0\,\text{A}$, it allows to minimize the AC Ampere-turn losses imposed by i^A along the x direction.

n^p and n^A are 252 and 20 respectively. The two auxiliary windings are connected so that they produce opposite magnetic fields when fed by i^A. That way, those fields cancel each other outside the area which covers a l_VAG length, qualified as "disturbed", around the auxiliary windings when the effects generated by v^p and i^A interact. Fig. 3b shows the magnetic field lines distribution for $i^\text{p} = 0\,\text{A}$ and Fig. 3c shows this distribution for $i^\text{A} = 20\,\text{A}$ and $V^\text{p} = 240\,\text{V}$ at a time step t such that $b^\text{p} = \hat{b}^\text{p} = 0.984\,\text{T}$, leading to $i^\text{p} = \hat{i}^\text{p} = 2.18\,\text{A}$. These field lines maps show that, on l_VAG, it is possible to distinguish two different states, noted High (H) and Low (L) levels. On the H level, at a given time step t such that $i^\text{p} > 0\,\text{A}$, the very large majority of the flux establishes between the orifices, whereas on the L level it establishes on the orifice external sides. This flux distribution is inverted at $t + T/2$. In order to distinguish the parameters depending on whether they are related to the High or Low level, they will be noted with a H or L index respectively. Similarly, in order to distinguish the parameters depending on whether they are related to interior or exterior areas, they will be noted with an "int" or "ext" index. Moreover, in the following, a lower index "0" is used to denote a variable when $i^\text{A} = 0\,\text{A}$.

III. Analytical Modeling

The modeling is based on the reluctance network presented in Fig. 4. $\epsilon^\text{p} = n^\text{p} i^\text{p}$ and $\epsilon^\text{A} = n^\text{A} i^\text{A}$ denote the magnetic excitations produced by the main winding and the auxiliary windings respectively. The plus (+) and minus (-) signs associated to ϵ^A refer to the previously stated magnetic opposition. The construction of the proposed reluctance network assumes magnetic flux circulating along the y axis inside the disturbed area. Then, three courses of action are possible to account for the distortions of field lines around the orifices' extremities along the x and x' axes:

- The first way to proceed assumes, considering the effects produced by ϕ^p generated by v^p, that the increasing of the field lines length generated by these distortions is negligible compared to the ones we would have established in the unmodified magnetic circuit. Hence, those distortions do not significantly affect the magnetic effects produced by this flux component. Then, only an adjustment of the DC Ampère-turns (At) is necessary by considering a useful magneto-motive force $\lambda_\text{A}\epsilon^\text{A}$ with $\lambda_\text{A} < 1$. Obtaining λ_A is done based on Fig. 3b by considering the mean flux tube and calculating the magnetic potential difference appearing on the tube's elements oriented along the y axis. This leads to a first approximation of λ_A as follows:

$$\lambda_\text{A} = \frac{\gamma(\gamma + c)}{\gamma(\gamma + c) + a(a + d)} \tag{1}$$

- The second way to proceed consists in characterizing the reluctances R_MCUA, R_int and R_ext which refer to the undisturbed magnetic core area, to the areas located inside and on the external sides of the auxiliary windings respectively, by considering the fictive heights $\frac{l_\text{VAG}}{2} = 2\gamma + c + d$ superior to the ones of the orifices. Given the symmetries, R_int and R_ext are each defined with a section equal to $2Da$.
- The third possibility consists in combining the two aforementioned methods and adjusting λ_A and γ in order, if necessary, to match the results of the analytic expressions with the measurements, for a given pair (i^A, V^p)

Actually, whichever chosen procedure, determining γ remains a problem. In order to numerically compute it, a finite element analysis is done to determine the axis x' position closest to the orifices for which the magnetic potential difference, along x', can be considered negligible.

The reluctance network presented in Fig. 4 is obtained using the third procedure. With $n^\text{A} = 20$ and a current density of $10\,\text{A}$ it leads to $a = 14.5\,\text{mm}$, $\gamma = 20\,\text{mm}$, $c = 20\,\text{mm}$ and $d = 4\,\text{mm}$. The rated i^A current is equal to $20\,\text{A}$.

Finally, to use the reluctance network shown in Fig. 4, the curve $\mu_\text{r}(b)$ has been linearized by portions as shown in Fig. 2. For the k^th straight line segment (SLS$_k$), μ_r is defined by:

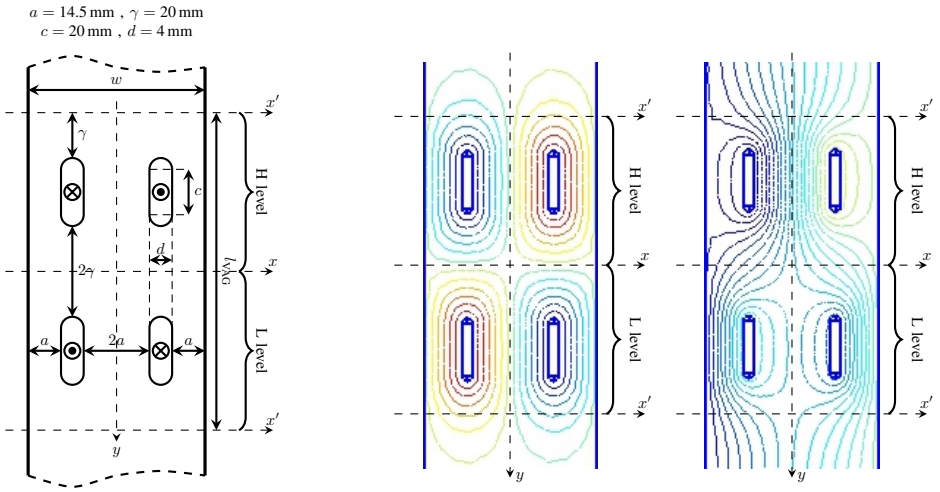

(a) Design of the VAG orifices

(b) Field lines for $i^{\text{A}} = 20\,\text{A}$ and $i^{\text{p}} = 0\,\text{A}$

(c) Field lines for $i^{\text{A}} = 20\,\text{A}$ and $i^{\text{p}} = 2.18\,\text{A}$

Fig. 3. Characterization of the disturbed area by the virtual air gap

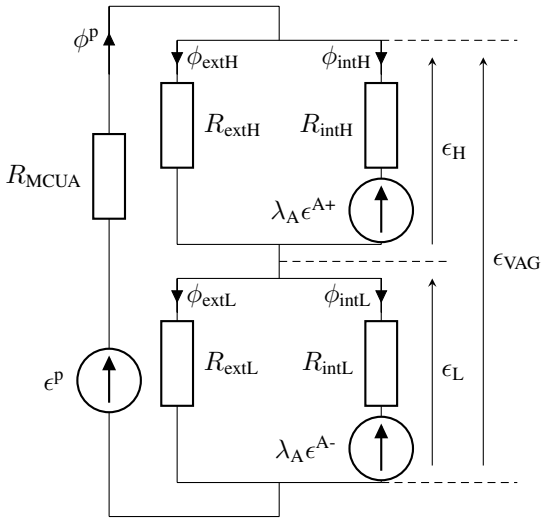

Fig. 4. Reluctance network

TABLE I
CHARACTERIZATION OF $\mu_{\text{R}}(b)$ BY STRAIGHT LINE SEGMENTS

k	α_k	β_k	b_{min} (T)	b_{max} (T)
1	6050	100	0	0.5
2	7627.75	−3055.55	0.5	0.86
3	10830.5	−6779.66	0.86	1.517
4	1372.55	−545.02	1.517	2.1

$$\mu_{\text{r}} = \alpha_k + \beta_k b \text{ for } b_{\text{min}\,k} < b < b_{\text{max}\,k} \tag{2}$$

Table I provides the values of α_k and β_k with respect to k.

Let us neglect the main winding voltage drop. At a given voltage source $v^{\text{p}} = \hat{v}^{\text{p}}\cos(\omega t)$ it comes $v^{\text{p}} = \frac{d\psi^{\text{p}}}{dt}$ where ψ^{p} is the main winding linked flux. Let us then assume that the generated AC magnetic flux ϕ^{p} is evenly distributed over the width w of the magnetic circuit in the undisturbed zone, it comes $\psi^{\text{p}} = n^{\text{p}}\phi^{\text{p}}$. Since $\phi^{\text{p}} = b^{\text{p}}S_{\text{MC}}$, it can be deduced:

$$b^{\text{p}} = \frac{\hat{v}^{\text{p}}}{n^{\text{p}}\omega S_{\text{MC}}}\sin(\omega t) \tag{3}$$

Considering the rule of flux conservation and neglecting leakage fluxes, the magnetic flux density b'^{p} in the disturbed area can be evaluated:

$$b'^{\text{p}} = b^{\text{p}}\frac{w}{4a} \tag{4}$$

Even if the values of b^{p} and b'^{p} are known at any time, their distribution in the disturbed area remains unknown. In this area, considering for example the flux between and on the sides of the orifices related to the H level, the following relations has to be satisfied:

$$\begin{cases} \phi^{\text{p}} = \phi_{\text{extH}} + \phi_{\text{intH}} \\ R_{\text{extH}}\,\phi_{\text{extH}} = \epsilon_{\text{H}} \\ R_{\text{intH}}\,\phi_{\text{intH}} + \lambda_{\text{A}}\epsilon^{\text{A+}} = \epsilon_{\text{H}} \end{cases} \tag{5}$$

where ϵ_H is the magnetic potential difference appearing on the H level terminals (Fig. 4). It can then be deduced:

$$b_{\text{extH}} + b_{\text{intH}} = 2b'^{\text{p}} \tag{6}$$

By assuming that the operating points located between and on the sides of the orifices belong to a k and a k' portion respectively, it comes:

$$\begin{cases} R_{\text{intH}} = \dfrac{1}{\mu_0(\alpha_k + \beta_k b_{\text{intH}})}\dfrac{w\,l_{\text{VAG}}}{4aS_{\text{MC}}} \\ R_{\text{extH}} = \dfrac{1}{\mu_0(\alpha_{k'} + \beta_{k'} b_{\text{extH}})}\dfrac{w\,l_{\text{VAG}}}{4aS_{\text{MC}}} \end{cases} \tag{7}$$

where μ_0 is the vacuum magnetic permeability. Combining (5) and (7) leads to:

$$\frac{b_{\text{extH}}}{(\alpha_{k'} + \beta_{k'} b_{\text{extH}})} - \frac{b_{\text{intH}}}{(\alpha_k + \beta_k b_{\text{intH}})} = \frac{2\mu_0}{L_{\text{VAG}}}\lambda_{\text{A}}\epsilon^{\text{A}} \tag{8}$$

Introducing (6) in (8) and defining the following parameters:

$$\begin{cases} K_{\rm A} = \dfrac{2\mu_0 \lambda_{\rm A} n^{\rm A}}{l_{VAG}} \\ N_1 = 2a(\beta_{k'} - \beta_k) \\ N_2 = -2a(\alpha_k + \alpha_{k'}) + b^{\rm p} w(\beta_k - \beta_{k'}) \\ N_3 = b^{\rm p} w \alpha_k \\ D_1 = -2a\beta_k \beta_{k'} \\ D_2 = 2a(\alpha_{k'}\beta_k - \alpha_k \beta_{k'}) + \beta_k \beta_{k'} b^{\rm p} w \\ D_3 = \alpha_k(2a\alpha_{k'} + \beta_k b^{\rm p} w) \end{cases} \tag{9}$$

the following relation can be deduced:

$$(N_1 - K_{\rm A} i^{\rm A} D_1) {b_{\rm intH}}^2 + (N_2 - K_{\rm A} i^{\rm A} D_2) b_{\rm intH} + (N_3 - K_{\rm A} i^{\rm A} D_3) = 0 \tag{10}$$

Setting:

$$\Delta = (N_2 - K_{\rm A} i^{\rm A} D_2)^2 - 4(N_1 - K_{\rm A} i^{\rm A} D_1)(N_3 - K_{\rm A} i^{\rm A} D_3) \tag{11}$$

leads to:

$$b_{\rm intH} = \frac{-(N_2 - K_{\rm A} i^{\rm A} D_2) \pm \sqrt{\Delta}}{2(N_1 - K_{\rm A} i^{\rm A} D_1)} \tag{12}$$

Then, one has to check if the values of $b_{\rm extH}$ and $b_{\rm intH}$ belong to the intervals delimiting the k and k' portions according to Table I. If not, another couple [k,k'] is chosen and the procedure if performed again until relevant values are found. Then, the same procedure is performed for the L level.

IV. Waveforms

The numerical exploitation of relations established in section III leads to the following equalities:

$$\begin{cases} R_{\rm intH} = R_{\rm extL} \\ R_{\rm extH} = R_{\rm intL} \end{cases} \tag{13}$$

$$\begin{cases} b_{\rm intH} = b_{\rm extL} \\ b_{\rm extH} = b_{\rm intL} \end{cases} \tag{14}$$

Fig. 5a shows the variations, on a period T, of $\delta v^{\rm p} = \frac{v^{\rm p}}{\hat{v}^{\rm p}}$, $b^{\rm p}$ and $i^{\rm p}$ for $i^{\rm A} = 20\,{\rm A}$, $V^{\rm p} = 240\,{\rm V}$ and $\lambda_{\rm A} = 1$. For comparison, this figure also shows the variation of $i_0^{\rm p}$. Figs. 5b and 5c give the variations of the magnetic potential differences $\epsilon_{\rm H}$, $\epsilon_{\rm L}$ and $\epsilon_{\rm VAG} = \epsilon_{\rm L} + \epsilon_{\rm H}$ appearing in the disturbed area as well as the variations of $b'^{\rm p}$, $b_{\rm intH}$ and $b_{\rm extH}$ respectively, during the same period. The variations of $i^{\rm p}$, $i_0^{\rm p}$, $\epsilon_{\rm H}$, $\epsilon_{\rm L}$ and $\epsilon_{\rm VAG}$ obtained from finite element computations are presented in Fig. 6. It can be noted that the reluctance network and the finite element computations lead to very similar results. It implicitly means that the second one of procedures stated in section III can be efficient, as a first approximation. Note that these waveforms can be qualified as "theoretical" because the effects of the main winding voltage drop are not taken into account and $i^{\rm A}$ is an absolutely perfect DC current. Curves shown in Figs. 5a and 6a confirm the VAG efficiency considering the amplitude variations of $i^{\rm p}$ compared to $i_0^{\rm p}$. Figs. 5b and 6b highlight that $\epsilon_{\rm VAG}$ is almost equal to $n^{\rm A} i^{\rm A}$ and $-n^{\rm A} i^{\rm A}$ when $b^{\rm p} > 0$ and $b^{\rm p} < 0$ respectively. Then, it is possible as a first approximation to characterize the VAG operation by the relation:

$$n^{\rm p} i^{\rm p} = R_{\rm MCUA} \phi^{\rm p} + n^{\rm A} i^{\rm A} {\rm sgn}(\phi^{\rm p}) \tag{15}$$

Since $l_{\rm VAG}$ is small (128 mm) compared to $L_{\rm MC}$ (1160 mm) it is possible to express relation (15) as follows:

$$n^{\rm p} i^{\rm p} = n^{\rm p} i_0^{\rm p} + n^{\rm A} i^{\rm A} {\rm sgn}(\phi^{\rm p}) \tag{16}$$

Since $R_{\rm MC}$ denotes the reluctance of the magnetic core seen from the primary winding, it comes: $\phi^{\rm p} = \frac{n^{\rm p} i^{\rm p}}{R_{\rm MC}}$. Moreover, since $\psi^{\rm p} = n^{\rm p} i^{\rm p}$ it is possible to evaluate the main winding inductance value $L^{\rm p} = \frac{{n^{\rm p}}^2}{R_{\rm MC}}$. The reluctance $R_{\rm g}$ of the mechanical equivalent air gap associated to the disturbed area is related to g as follows:

$$g = \mu_0 S_{\rm MC} R_{\rm g} \tag{17}$$

Then, the value of $R_{\rm g}$ can be calculated by comparing the values of $\phi^{\rm p}$ and $\phi_0^{\rm p}$. Assuming that $g << L_{\rm MC}$ leads to the equality $R_{\rm MC} = R_{\rm MC_0} + R_{\rm g}$ allowing to compute the value of g. Fig. 7 show the variations of $L^{\rm p}$, $L_0^{\rm p}$ and g with time during a period T. $b^{\rm p}$ is also shown in Fig. 7 in order to better find the position of the extrema of the deduced quantities which present quite disturbed variations that do not allow an easy pre-designing phase.

V. Characteristics and Experimental Checks

The following experimental checks concern the magnetic core designed in section III. Moreover, since the evolution laws of certain parameters are relatively complex, the following developments consider their fundamental component only. The latters are noted with a "(1)" index.

In order to propose a more suitable designing tool let us note $i^{\rm p}_{\rm (rms)}$ the equivalent sinusoidal current associated to $i^{\rm p}$. By definition, those $i^{\rm p}_{\rm (rms)}$ and $i^{\rm p}$ have the same RMS value. In the cases considered in Figs. 5 and 7 the fundamental peak value of $i^{\rm p}$ is $\hat{i}^{\rm p}_{(1)} = 2.455\,{\rm A}$. Moreover, $I^{\rm p} = 1.767\,{\rm A}$ leads to $\hat{i}^{\rm p}_{\rm (rms)} = 2.498\,{\rm A}$. About $i_0^{\rm p}$, the computed values are $\hat{i}^{\rm p}_{0(1)} = 0.606\,{\rm A}$ and $\hat{i}^{\rm p}_{0({\rm rms})} = 0.611\,{\rm A}$. The difference between the peak values is less than 2 % for $i^{\rm p}$ and around 1 % for $i_0^{\rm p}$. Then the errors made when using $i^{\rm p}_{\rm (rms)}$ instead of $i^{\rm p}$ are compatible with the assumptions necessarely made to perform this analytical study.

Since only sinusoidal quantities are considered, the relations previously stated for the determination of $L^{\rm p}$ and g instantaneous values lead to characterize those quantities by their mean values $< L^{\rm p} >$ and $< g >$ which present a constant value during a period T:

$$< L^{\rm p} > = \frac{\hat{v}^{\rm p}}{\hat{i}^{\rm p}_{\rm (rms)} \omega} \tag{18}$$

$$< g > = \mu_0 \, S_{\rm MC} \, {n^{\rm p}}^2 \, \frac{\omega}{\hat{v}^{\rm p}} \, (\hat{i}^{\rm p}_{\rm (rms)} - \hat{i}^{\rm p}_{0({\rm rms})}) \tag{19}$$

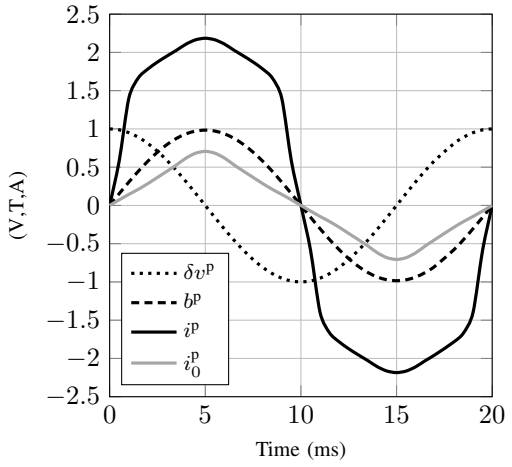

(a) δv^{p}, b^{p}, i^{p}, i_0^{p}

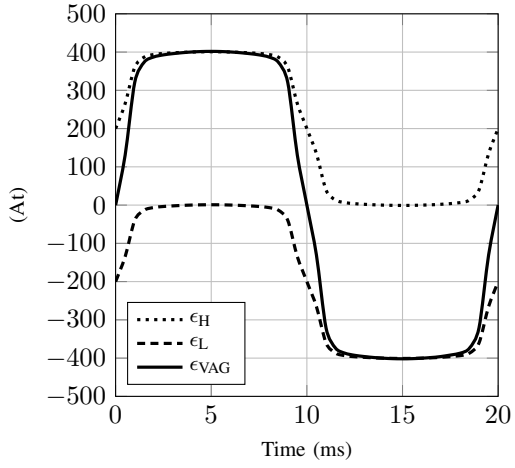

(b) ϵ_{H}, ϵ_{L}, ϵ_{VAG}

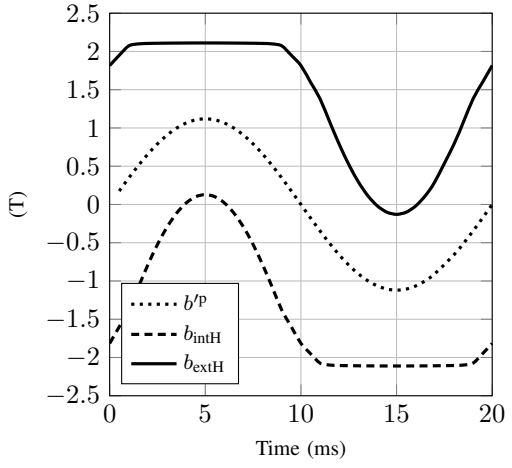

(c) b'^{p}, b_{intH}, b_{extH}

Fig. 5. Variations with time of the main electric and magnetic variables for $V^{\mathrm{p}} = 240\,\mathrm{V}$ and $i^{\mathrm{A}} = 20\,\mathrm{A}$

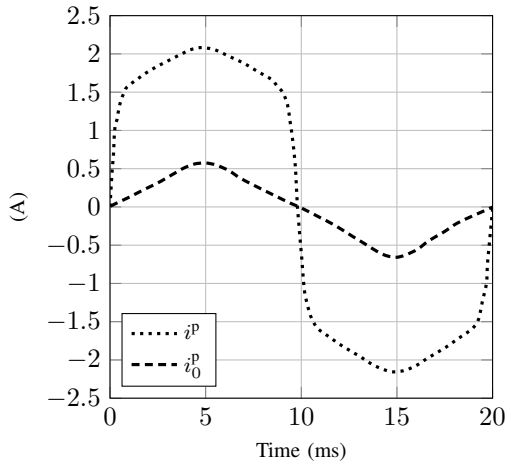

(a) i^{p} and i_0^{p}

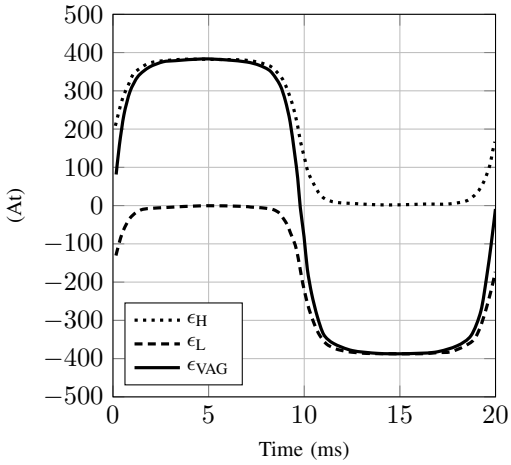

(b) ϵ_{H}, ϵ_{L}, ϵ_{VAG}

Fig. 6. Variations with time (finite element computation) of i^{p}, i_0^{p}, ϵ_{H}, ϵ_{L} and ϵ_{VAG} for $V^{\mathrm{p}} = 240\,\mathrm{V}$ and $i^{\mathrm{A}} = 20\,\mathrm{A}$

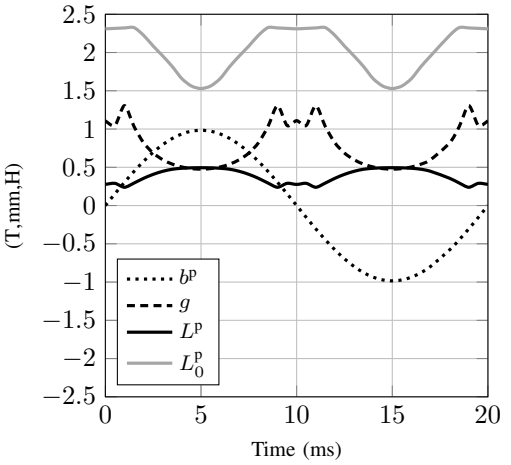

Fig. 7. Variations with time of b^{p}, g, L^{p}, L_0^{p} for $V^{\mathrm{p}} = 240\,\mathrm{V}$ and $i^{\mathrm{A}} = 20\,\mathrm{A}$

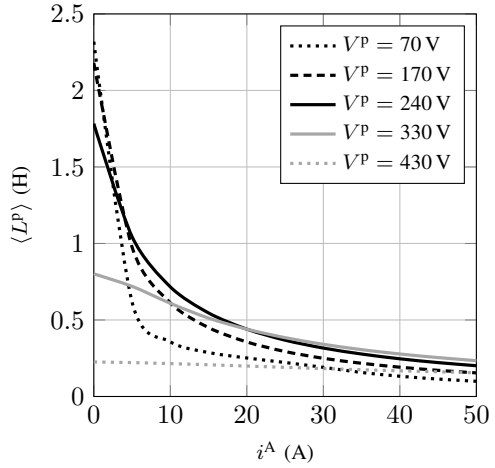

(a) Variations of $\langle L^{\mathrm{p}} \rangle$ with i^{A}

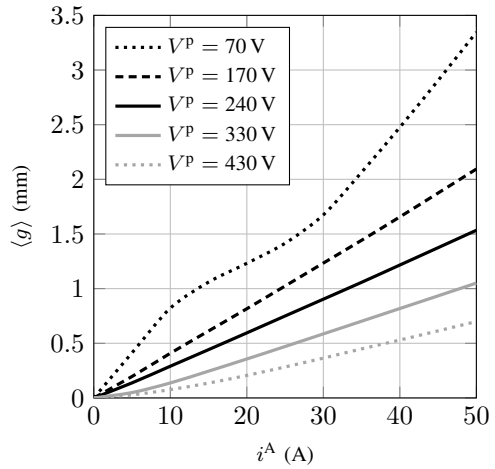

(b) Variations of $\langle g \rangle$ with i^{A}

Fig. 8. Variations with i^{A} of external characteristics for $V^{\mathrm{p}} = 70\,\mathrm{V}$, 170 V, 240 V, 330 V and 430 V

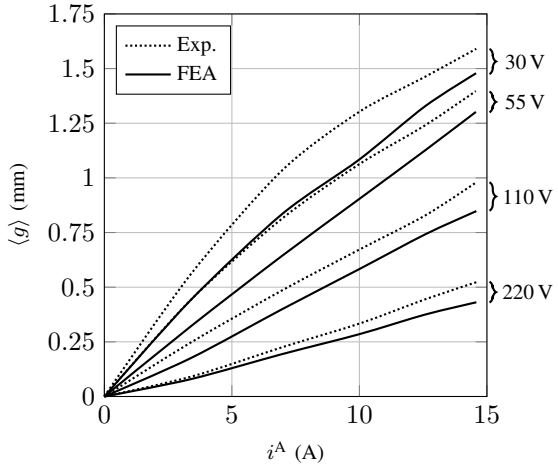

(a) Determination for various V^{p}

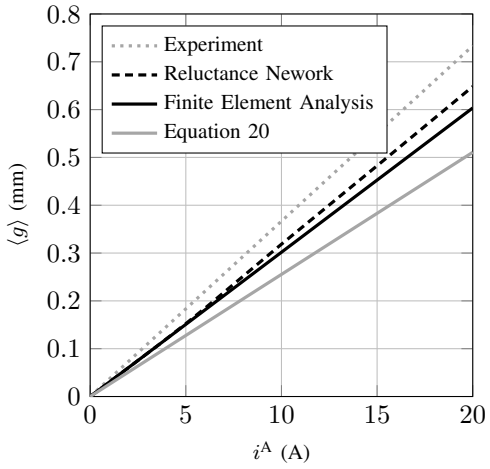

(b) Determination for $V^{\mathrm{p}} = 220\,\mathrm{V}$

Fig. 9. Variations of $\langle g \rangle$ with i^{A} for various conditions

Fig. 8 shows the theoretical variations of $< L^{\mathrm{p}} >$ (Fig. 8a) and $< g >$ (Fig. 8b) deduced from (18) and (19), for several values of V^{p} chosen so that for $i^{\mathrm{A}} = 0$ the operating point is:

- around the middle of SLS_1: $V^{\mathrm{p}} = 70\,\mathrm{V}$, $\hat{b}^{\mathrm{p}} = 0.3\,\mathrm{T}$,
- around the middle of SLS_2: $V^{\mathrm{p}} = 170\,\mathrm{V}$, $\hat{b}^{\mathrm{p}} = 0.7\,\mathrm{T}$,
- on the upper level of SLS_3: $V^{\mathrm{p}} = 240\,\mathrm{V}$, $\hat{b}^{\mathrm{p}} = 1\,\mathrm{T}$,
- on the lower level of SLS_3: $V^{\mathrm{p}} = 330\,\mathrm{V}$, $\hat{b}^{\mathrm{p}} = 1.35\,\mathrm{T}$,
- around the middle of SLS_4: $V^{\mathrm{p}} = 430\,\mathrm{V}$, $\hat{b}^{\mathrm{p}} = 1.8\,\mathrm{T}$.

Fig. 8b shows the efficiency of the VAG by highlighting that the performances in terms of equivalent air gap thickness increase with i^{A} and decrease with V^{p}. This result was expected since for high values of V^{p} the saturation affects the whole magnetic core.

The experimental measurements about $< g >$ come from several papers already published. Fig. 9a, taken from [12], shows the variations of $< g >$ with i^{A} for several values of V^{p} (30 V, 55 V, 110 V, 220 V), as well as the results obtained from a finite element analysis. Let us point out that the magnetic core used in [12] is the same as the one described in this paper. Only the geometry of the auxiliary windings orifices differs. Moreover, the considered magnetic core includes two VAG instead of one in order to validate that the principle of summation of the VAG magnetic effects. Consequently, since the values of n^{p} and n^{A} are identical, the scale of the y-axis of the curves presented in [12] was adapted (division by 2) to obtain Fig. 9a. By comparing Fig. 8b with Fig. 9a it can be noted that despite the differences between the two structures, the results given by the analytical model presented in this paper are in good accordance with those obtained experimentally using the concept of equivalent sinusoidal current. For example, $< g >$ is of the order of 5 mm for $i^{\mathrm{A}} = 15\,\mathrm{A}$ when V^{p} is close to 220 V. This is indeed remarkable since, from an experimental point of view, the assumptions made about the main winding voltage drop and the ideal i^{A} current are no longer satisfied. In order to make a rigorous comparison, the proposed model has been used at $V^{\mathrm{p}} = 220\,\mathrm{V}$. Fig. 9b shows the variations of $< g >$ with i^{A} obtained experimentally - deduced from [12] - by the reluctance network proposed in this paper, by finite element analysis and by (20), the latter allowing to determinate an approached value of $< g >$ deduced from (19) and (16) by substituting $n^{\mathrm{A}} i^{\mathrm{A}}$ with $n^{\mathrm{p}}(\hat{i}^{\mathrm{p}}_{(\mathrm{rms})} - \hat{i}^{\mathrm{p}}_{0(\mathrm{rms})})$:

$$< g >= \mu_0 \, S_{\mathrm{MC}} \, n^{\mathrm{p}} n^{\mathrm{A}} \, \frac{\omega}{\hat{v}^{\mathrm{p}}} \, i^{\mathrm{A}} \tag{20}$$

It appears that all the methods underestimate the value of $< g >$. Moreover, the maximum difference between experiments and (20) is up to 30 %, for $i^{\mathrm{A}} = 20\,\mathrm{A}$, whereas the results given by the reluctance network are in good accordance with experiments. Then, if the aim of a study is to quickly obtain a first sizing, then one can use relation (20). If the study needs more accuracy, then the reluctance network should be used. Of course, it is still possible to model the whole structure using the finite element method, but this method is too time consuming for a design purpose.

VI. Conclusion

The purpose of this study is to propose a pre-designing tool of a device including a virtual air gap. This tool has been realized following several reflexions that came to us following the analysis of one-phase as well as three-phase real cases. The methodology consists in designing, in a first step, a magnetic core assuming that actual mechanical air gaps, with variable thickness, are inserted in it. In a second step, knowing the boundaries of this thickness allow to characterize the auxiliary windings and orifices, keeping in mind that it has to be technically buildable. In order to optimize the structure, this tool is able to quickly answer to questions such as: What is the impact of the orifice shapes on the results? What is the impact of the electrical steel grade on the virtual air gap performances? In the case of the use of grain oriented electrical steel, is it better to use the rolling direction or the transverse direction? Of course, final fine tuning of the design can still be performed using finite element simulations but the flexibility of the presented tool makes it an interesting alternative.

References

[1] V. Molcrette, J.-L. Kotny, J.-P. Swan, and J.-F. Brudny, "Reduction of inrush current in single-phase transformer using virtual air gap technique," *IEEE Transactions on Magnetics*, vol. 34, no. 4, pp. 1192–1194, Jul. 1998.

[2] D. S. L. Dolan and P. W. Lehn, "Harmonic mitigation in a virtual air gap variable reactor via control current modulation," in *Power and Energy Society General Meeting - Conversion and Delivery of Electrical Energy in the 21st Century, 2008 IEEE*, July 2008, pp. 1–5.

[3] S. Magdaleno and C. Rojas, "Control of the magnetizing characteristics of a toroidal core using virtual gap," in *Electronics, Robotics and Automotive Mechanics Conference (CERMA)*, Sep. 2010, pp. 540–545.

[4] J. Avila-Montes and E. Melgoza, "Scaling the virtual air-gap principle to high voltage large power applications," in *Electrical Machines (ICEM), XXth International Conference on*, Sep. 2012, pp. 757–762.

[5] J. Avila-Montes, D. Campos-Gaona, E. M. Vàzquez, and J. R. Rodríguez-Rodríguez, "A novel compensation scheme based on a virtual air gap variable reactor for ac voltage control," *IEEE Transactions on Industrial Electronics*, vol. 61, no. 12, pp. 6547–6555, Dec 2014.

[6] A. Konrad and J.-F. Brudny, "An improved method for virtual air gap length computation," *IEEE Transactions on Magnetics*, vol. 41, no. 10, pp. 4051–4053, Oct. 2005.

[7] J.-F. Brudny, P. Guuinic, and V. Costan, "Series current limiter using a magnetic circuit comprising holes and windows," Patent, 2012, WO 2012/126886.

[8] P. Guuinic, J.-F. Brudny, V. Costan, and M. Dessoude, "Series voltage regulator with electronics protected against short-circuits by magnetic circuit-based decoupling using holes and windows," Patent, 2012, WO 012/126884.

[9] V. Majchrzak, G. Parent, J.-F. Brudny, V. Costan, and P. Guuinic, "Coupling transformer with a virtual air gap for the protection of dynamic voltage restorers," in *IECON 2014 - 40th Annual Conference of the IEEE Industrial Electronics Society*, Nov. 2014, pp. 462–468.

[10] ——, "Design of a coupling transformer with a virtual air gap for dynamic voltage restorers," *IEEE Transactions on Magnetics*, vol. 52, no. 7, pp. 1–4, Jul. 2016.

[11] M. Moallem and G. E. Dawson, "An improved magnetic equivalent circuit method for predicting the characteristics of highly saturated electromagnetic devices," *IEEE Transactions on Magnetics*, vol. 34, no. 5, pp. 3632–3635, Sep 1998.

[12] A. Konrad and J.-F. Brudny, "Virtual air gap length computation with the finite-element method," *IEEE Transactions on Magnetics*, vol. 43, no. 4, pp. 1829–1832, Apr. 2007.